


Article

Retrofit Proposals for Energy Efficiency and Thermal Comfort in Historic Public Buildings: The Case of the Engineering Faculty's Seat of Sapienza University

Andrea Vallati, Miriam Di Matteo and Costanza Vittoria Fiorini * 

DIAEE—Department of Astronautical, Electrical and Energy Engineering, Sapienza University of Rome, Via Eudossiana 18, 00184 Rome, Italy

* Correspondence: costanzavittoria.fiorini@uniroma1.it

Abstract: The building sector greatly contributes to energy consumption and Greenhouse Gas emissions, relating to the whole building life cycle. Boasting a huge building heritage of historical and architectural value, Europe faces challenging retrofit perspectives, as the potential for high energy efficiency has to be exploited while preserving the buildings' original characteristics. The present work aims to feature the influence of a passive strategy on a heritage building in a mild climate. As historical its façade cannot be modified, its large glazing areas involve multiple issues, such as an increase in the heating (Q_H) and cooling (Q_C) energy demands and the risk of thermal discomfort. Thus, window replacement was proposed for retrofitting. A dynamic simulation model in TRNSYS was validated with experimental data collected by the continuous monitoring of walls of different thicknesses and orientations. Solutions from replacement with Double Glazing Units (DGUs) with improved thermal insulation, to internal shading activation were applied. All configurations were compared in terms of Q_H , Q_C , thermal performance of the building and user comfort (Fanger). Low-e DGU enabled the saving of up to 14% of the annual energy demand, and shading also offered good results in summer, reducing Q_C by 19%. In summer, DGU involved a maximum PPD reduction of 10 units.



Citation: Vallati, A.; Di Matteo, M.; Fiorini, C.V. Retrofit Proposals for Energy Efficiency and Thermal Comfort in Historic Public Buildings: The Case of the Engineering Faculty's Seat of Sapienza University. *Energies* **2023**, *16*, 151. <https://doi.org/10.3390/en16010151>

Academic Editors:
Małgorzata Basińska and
Katarzyna Ratajczak

Received: 25 October 2022
Revised: 30 November 2022
Accepted: 4 December 2022
Published: 23 December 2022



Copyright: © 2022 by the authors. Licensee MDPI, Basel, Switzerland. This article is an open access article distributed under the terms and conditions of the Creative Commons Attribution (CC BY) license (<https://creativecommons.org/licenses/by/4.0/>).

Keywords: historic buildings; microclimatic monitoring; dynamic simulation; energy efficiency; HVAC systems

1. Introduction

The building sector is one of the main contributors to energy consumption and Greenhouse Gas (GHG) emissions. According to the European Commission, in 2014 the energy involved in operating heating, cooling, ventilation and artificial lighting is responsible for between 40% and 70% of the total building energy consumption [1] and a large percentage, around 55%, is in charge of the heating and cooling system [2]. Improving the environmental footprint of the existing building stock, in terms of energy demand, thus represents a key strategy to be pursued. Europe boasts a building heritage characterized by a significant number of old buildings of high historical, architectural and cultural value, increasing the energy efficiency of which represents a challenging issue, since the sustainable retrofit has to also achieve the preservation of the building's original characteristics.

The design phase in refurbishment projects is often problematic; historical buildings present many artistic and architectural constraints that make the problem difficult [3], especially in the application of envelope refurbishment measures. Therefore, even more than in modern buildings, it is necessary to focus efforts on their efficiency. Plant efficiency, and the application of alternative and renewable energy supply systems purposed for modern constructions and common retrofit, has not generally been fully explored for historical buildings [4]. In [5], Heat Pump (HP) typologies exploiting different renewable sources (air, water, ground), and control systems for heating and cooling (economic and

energy needs) in a historical house were compared. The energy analysis showed that the inverter-driven Ground Coupled Heat Pump (GCHP) was the most convenient solution among those analyzed, since it had the lowest annual requirement of primary energy from non-renewable sources (66,297 kWh/year). Emmi et al. [6] demonstrated that the use of low enthalpy geothermal energy as a heat source/sink for the HP was very promising, confirming that HPs able to increase the supply of high temperature at the condenser side make this technology suitable for their application in buildings characterized by low thermal insulation and high thermal capacity, such as historical buildings.

Passive retrofit is, however, the most commonly adopted strategy for existing buildings, with direct intervention on the weakest element [7]. Energy performance has been widely assessed considering the substitution of frame and glasses, external infills and the insulation of the roof and ground floor using green building concepts [8,9].

In historical buildings it is quite common to observe scarce thermal parameters for walls: in case they have very low thermal mass they are responsible for contained thermal shifts and low values of internal areal heat capacity [10]. Even outdated windows are a penalizing element for the building envelope, especially when Window-to-Wall Ratio (WWR), amount often significative of the building construction period, is high [11].

Intervening on windows means acting on an element which is responsible for a significant portion of undesired thermal loss or gain in a building, and at the same time does not involve the external façade being modified [8].

This has led to increasingly stringent recommendations and regulations for both new constructions and the retrofitting of older buildings, alongside a technological improvement of the element itself [12]. Jelle et al. [13,14] extensively reviewed current fenestration technologies from double- and triple-pane windows, to vacuum glazing and low-emissivity coatings, to photochromic glass and smart windows.

Proposing the use of low solar heat gain glasses for a public historical building in a hot-humid climate, and assessing it in combination with other passive and active retrofit solutions by a validated dynamic model, Ozbalta et al. [3] confirmed that low Solar Heat Gain Coefficient (SHGC) glasses represent a measure that greatly improves energy consumption (from 0.96% to 1.19%) and global costs. Pereira et al. [15] proposed Solar Control Films (SCFs) as a passive retrofitting solution for single-glazed windows, analyzing through an EnergyPlus simulation model experimentally validated, how to change their solar-optical properties, in order to reduce solar gains and energy use and to increase indoor comfort conditions. The reduction of solar gains involves a decrease in the cooling energy use for South, East and West orientations, while there is an increase in the heating and lighting energy use; when compared to the bare single clear glass, the glass with the SCF reduces the average indoor temperature during working hours in both the winter and summer seasons, with a maximum percent reduction during summer days (14.7%), two times larger than that of winter days (7.1%).

However, often, fenestration retrofitting is interpreted as window replacement, whilst the energy-saving potential allowed by window maintenance or non-destructive measures is rarely investigated. In [16], the validity of different retrofitting measures was assessed in terms of their long-term Life Cycle (LC) operating energy saving potential. Considering their performance obsolescence, it was demonstrated that destructive retrofitting techniques (such as window replacement) did not necessarily allow for the largest energy savings. Among window-maintenance strategies, the introduction of shading is also one of the preferred interventions in the case of historic buildings, when partial solutions are preferred to integral ones [17,18].

Moreover, control strategies must be properly evaluated, knowing that shading affects energy demand, especially in warm to hot climates [19], simultaneously influencing thermal and visual comfort. The integration of these two aspects represents a lack in Building Simulation Programs (BSP), in terms of inaccuracy and computational intensiveness, so much that methods to optimize input in dynamic BSP have become a topic of interest

over the years, from accurate time series for solar loads generation [20] to glare predictive models using machine learning algorithms developed from pre-simulated data [21].

The influence of different glazing types and exposures on thermal comfort and energy performance of a lecture room in a non-residential building was evaluated in [22] by experimental investigation and numerical analysis in unsteady-state conditions. Two codes, TRNSYS and EnergyPlus were compared, considering both the Direct Root Finding (DRF) method, with the former, and the State-Space method, with the latter. In mid-season from South to East orientation, the Predicted Percentage of Dissatisfied (PPD) ranged from 37% to 13% for a double-glazed window with a total area of 14.00 m² in a room of about 340 m². The two simulation codes results were in good agreement; small differences were attributed to the different approach for the evaluation of solar irradiance on tilted surfaces and to the transient heat conduction model.

Analyzing buildings inserted in an urban context, as is usually the case for historical buildings, even more public, also implies that the influence of the surrounding environment on the energy demand for space cooling and heating [23,24] should be taken into account, including the shading effect of nearby buildings.

To assess their complex hygrothermal behavior and possible strategies for their conservation, and to evaluate the suitability of energy retrofit scenarios, building dynamic simulation tools (traditionally used to study the hygrothermal performance of new buildings) have recently been adopted in historical buildings. The most widespread are EnergyPlus (26%), DesignBuilder (22%), TRNSYS (15%), and Wufi Plus (12%). Lack of reliable thermophysical input data for various envelope components, as well as intrinsic limitations in the models, compromises the accuracy of the results of these simulation software tools when employed for such a specific purpose [25]. The customization of modeling tools for recent buildings results in oversimplification, overlooking elements of the past architectural language, such as basements, columns, frames, portals, cornices and the shape of windows; this affects thermal results by underestimating the not negligible thermal bridging effects, or by introducing errors in the interpretation of the results. Among the most significant intrinsic limitations are those relating to heat and mass transfer processes [26]. In addition, the collection of stratigraphy data can very often be difficult, and several assumptions must be made. The optimization of the geometric and constructive model is therefore a fundamental node to bridge the discrepancy between actual performance and simulations.

Furthermore, the ISO 7730 assessment method [27] is often integrated with simulations in order to evaluate the comfort level in terms of Fanger's indices: Predicted Mean Vote (PMV) and Predicted Percentage of Dissatisfied (PPD). The Predicted Mean Vote takes into account temperature, humidity, air movement, clothing and metabolic activity. It is a thermal scale that spans from -3 (Very Cold) to $+3$ (Very Hot). Acceptable values lie between ± 1 , but the recommended comfortable PMV range is within ± 0.5 . Predicted Percentage of Dissatisfied is another thermal comfort index complementing PMV, to which it relates; as PMV changes from zero in either a positive or negative direction, PPD increases. Recent studies have highlighted the inaccuracy of PMV in predicting the observed thermal sensation in absolute terms, increasing towards the ends of the thermal sensation scale [17,28]. In addition, if the PMV model would perfectly predict thermal sensation, then PPD accuracy would be higher close to neutrality, but it would overestimate dissatisfaction by approximately 15–25% outside of it. Moreover, PMV-PPD accuracy varies strongly between ventilation strategies, building types and climate groups. To establish quantitative indices for supporting adaptive models in indoor thermal comfort evaluation, a correlation between experimental data measured by the instruments and subjective responses given by the occupants in different seasons and climatic zones was suggested, coupling Fanger and Wray comfort indices [29]. However, even if their performance is a contested topic, PMV and PPD remain the most widely used thermal comfort indices, representative for comparative qualitative analysis. They can therefore be satisfactorily adopted as indicators of passive action for public building refurbishment [10,11,30,31].

The present work aimed to feature the advantage of passive strategies and to analyze their influence on the indoor comfort level of a heritage building located in a mild climate. An interdisciplinary methodology was employed to evaluate the construction's conservation conditions and propose refurbishment and restoration interventions, on the basis of which to apply an experimental and numerical approach. The case study is the historical seat of the Faculty of Engineering of Sapienza University of Rome. The four-story construction was born as a conventual complex, became a university seat in 1873, and is listed as cultural property of the city, meaning that the external façade cannot be modified. The presence of large glazing areas there creates multiple issues, such as heat gain and heat loss, which increases the risks of thermal discomfort of occupants and the energy demands for space cooling and heating. Aiming to improve the thermal performance of the building, the replacement of the windows was proposed as a retrofitting solution, which avoids compromising the original façades.

From the energetic side, the development of this research followed mainly four phases:

- First phase: the thermal parameters (indoor and outdoor air temperature and thermal flux) of the external walls of the building in the original state were monitored. Measurements were made continuously on walls with different orientations, located on different floors, and with different thicknesses and stratigraphies.
- Second phase: data experimentally obtained, in addition to characterizing the building, enabled the validation of a dynamic simulation model created by TRNSYS Software, focusing the left wing of the building.
- Third phase: dynamic simulations of the building in the original state and in the energy efficient versions were performed, after the deployment of different glazing systems. Solutions from replacement with Double Glazing Units (DGUs) (with improved performance in terms of thermal insulation) to internal shading activation were applied. The behavior of the building before and after the hypothesized retrofit interventions was assessed in terms of energy loads and heating and cooling energy demand. For the analysis of the outcomes at the building level, internal air temperature and internal and external surface temperatures of the glass (T_{sig} and T_{seg}) were considered, in order to detail the influence of the building envelope on the global thermal performance.
- Fourth phase: the thermal performance of the building and the comfort of the users in the original and the improved configuration were compared; the parameters chosen as evaluation indicators were Fanger's PMV and PPD indices.

The implemented unsteady-state model represents a powerful tool in building design: many different solutions can be investigated, and the most appropriate design option can be selected from the simulation results.

2. Materials and Methods

2.1. Case Study

The framework is that of the historical seat of the Faculty of Engineering of Sapienza University of Rome, leaning against the Paleochristian Basilica (440 A.D.) of S. Pietro in Vincoli. The changes in the intended use of the building, from the original conventual complex to the current university seat, implied a series of functional adaptations, culminating in the planned extension of the end of the 1800 which was followed by continuous changes; substantial but without an organic project.

The building object of the work is the Eastern wing of the Engineering Faculty seat of Sapienza University of Rome, realized in 1766 as an extension of the complex, intended for hosting the library (Figure 1). The building has a rectangular footprint (22 m long and 12 m wide) and originally constituted two noble floors beyond the ground floor, with as many orders of windows. The spaces were later lowered by inserting intermediate slabs, constructed interrupting the continuity of the windows, which allowed the building to obtain two more floors. The current configuration comprises five levels above ground, of different ceiling heights, between 3.00 m and 5.20 m. The "typological" floor (second-floor) has a total volume of about 1135 m³. The rooms on the first floor are intended for

classrooms and laboratories, those on the upper floors are used as offices, while the ground floor is currently unused. Except for the latter, the floors are all heated. Only the North-East side and the upper part of the South-East façade are inner walls. The ground level has no openings to the outside, while all the other floors are characterized by four windows on the North-West side, two on the South-East side and one on the South-West side, except for the first floor. The windows of the even floors are very wide and with an arched shape, and those of the odd floors, rectangular and ribbon-shaped; although smaller in size, they extend continuously on the façades. The total Window-to-Wall Ratio is 13%. The current glazing system is a single glass layer 4 mm thick, and the frame is made of galvanized steel 0.0062 m thick. The opaque envelope's stratigraphy is made by a layer of full bricks and plaster mortar, of different thicknesses at the pilasters or at portions above or below the window, with internal and external finishing in lime gypsum plaster. There is no insulating layer. The ground floor is cast in place directly on the ground.

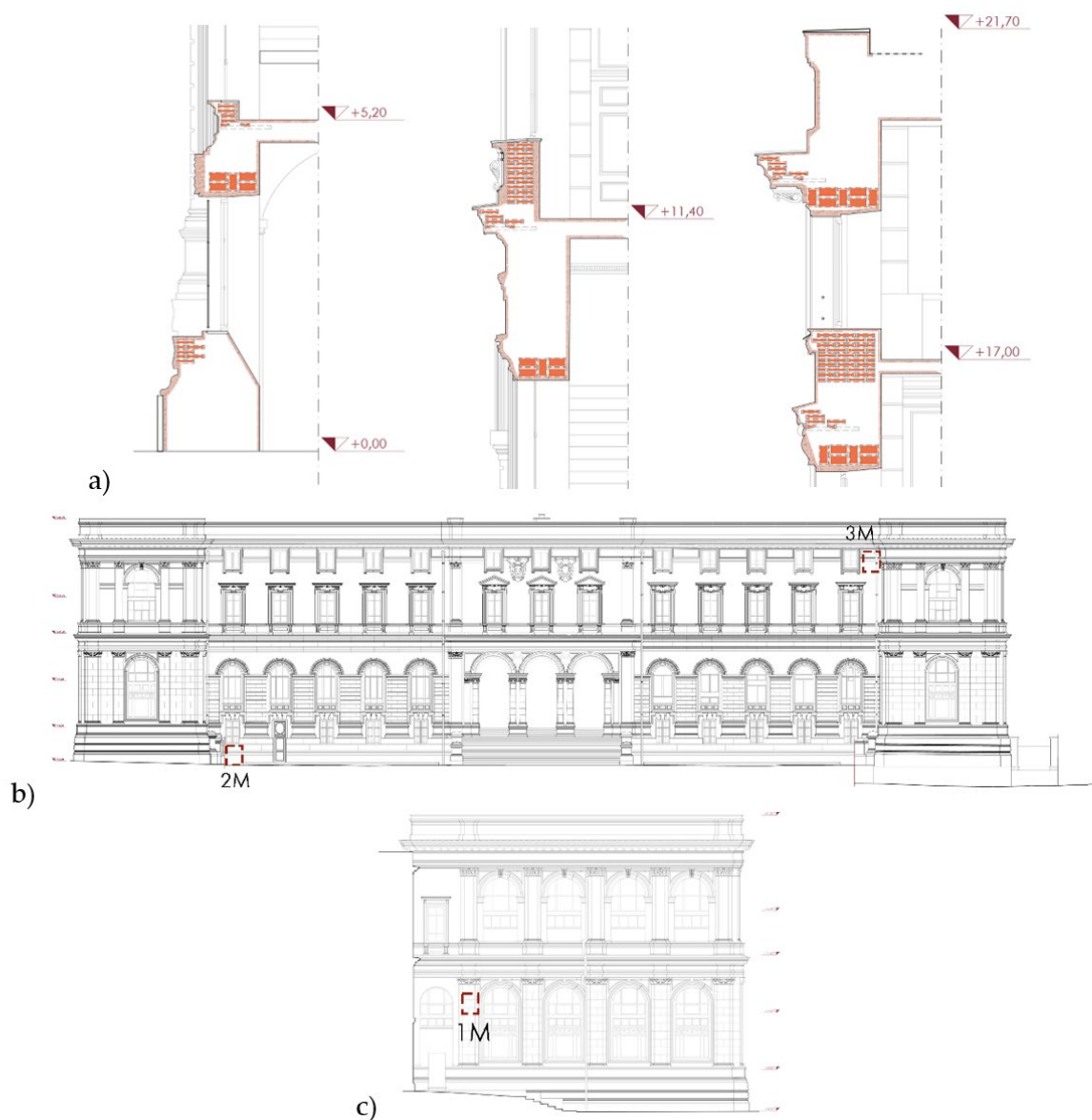


Figure 1. Case study. Investigated wall: Northern façade (b), Eastern façade (c) and particular of the stratigraphy (a).

In Table 1 the envelope's features are reported for each floor and orientation.

Table 1. Characteristics of the envelope.

Floor	N-O			S-O			S-E		
	Opaque Area [m ²]	Window Area [m ²]	WWRs [%] *	Opaque Area [m ²]	Window Area [m ²]	WWRs [%] *	Opaque Area [m ²]	Window Area [m ²]	WWRs [%] *
Fourth	114.3	21.2	19	62.7	5.3	8	69.0	10.6	15
Third	73.0	8.1	11	40.0	4.3	11	44.2	4.1	9
Second	92.9	15.3	16	50.9	3.8	8	56.1	7.7	14
First	92.9	4.7	5	50.9	0.0	0	56.1	2.4	4
Ground	66.3	0.0	0	36.4	0.0	0	40.1	0.0	0

* WWRs = Specific Window-to-Wall Ratio: fraction of gross exterior wall area occupied by windows, referred to a specific façade portion.

2.2. Experimental Campaign

Thermal parameters, i.e., the indoor and outdoor air temperature and thermal flux of the external walls of the building in the original state, were measured. Three subsequential continuous monitoring campaigns, each lasting about three days, were carried out in the winter of 2021 on walls of different orientation, floor location, thickness and stratigraphy (Figure 2) (Table 2). The first measuring point (M1) was located on the second floor, obtained from a later division of the original volume of the first floor, in correspondence with a pilaster; it had a thickness of 1.30 m and was North oriented. The second measuring point (M2) belonged to the basement, 1.40 m thick and facing East; the third investigated wall (M3) was placed on the main façade, facing West, at the height of the fourth floor and it was 1.20 m thick (Figure 1). During the investigation, conducted midweek, the rooms had a normal presence of people and the HVAC system was operational.



Figure 2. Indoor thermal conditions monitoring: M1 (a), M2 (b), M3 (c).

Table 2. Dimensions and thermophysical characteristics of the investigated façades: M1 (a), M2 (b), M3 (c).

(a) M1			
Materials	<i>s</i> m	λ W/(mK)	R_j (m ² K)/W
External laminar layer			0.130
External plaster	0.05	0.7	0.071
Solid brick	1.14	0.8	1.425
Internal plaster	0.05	0.7	0.071
Internal laminar layer			0.040
Global heat transfer coefficient (<i>U</i>) [W/(m²K)]			0.575
(b) M2			
Materials	<i>s</i> m	λ W/(mK)	R_j (m ² K)/W
External laminar layer			0.130
External plaster	0.05	0.7	0.071
Roman travertine	0.42	3.0	0.140
Solid brick	0.85	0.8	1.063
Internal plaster	0.05	0.7	0.071
Internal laminar layer			0.040
Global heat transfer coefficient (<i>U</i>) [W/(m²K)]			0.660
(c) M3			
Materials	<i>s</i> m	λ W/(mK)	R_j (m ² K)/W
External laminar layer			0.130
Solid brick	1.15	0.8	1.438
Internal plaster	0.05	0.7	0.071
Internal laminar layer			0.040
Global heat transfer coefficient (<i>U</i>) [W/(m²K)]			0.596

Data acquisition was performed using the Heat Flow Meter TESTO 435. The device consisted of a heat-flow plate for heat flux measurements, and two thermal probes for internal and external air temperature collection. The heat-flow sensor needed to be stuck to the inner side of the building envelope in a representative part of the wall. Effects related to cold bridges were avoided as they would potentially be responsible for errors that could affect the measurements; therefore, areas near corners and zones influenced by irregularities were excluded. The thermal sensors were made to be placed in correspondence with the heat-flow plate, on the two opposite sides of the investigated wall. The device automatically applied the Heat Flow Meter (HFM) method, following the ISO 9869–1 [32] standard, recording the global heat transfer coefficient (U , W/(m²K)) derived from heat fluxes (q_m) and indoor ($T_{i,m}$) and outdoor ($T_{e,m}$) air temperature measurements. The sampling rate for each probe was 10 min. The progressive average method was applied to determine the stationary U :

$$U = \frac{\sum_{j=1}^N q_{m,j}}{\sum_{j=1}^N (T_{i,m,j} - T_{e,m,j})} \quad (1)$$

where j is for the j -th measured value and N represents the overall recorded samples.

In Figure 3, the measured global heat transfer coefficient trends of the examined façades are reported. Looking at Figure 3a, the negative U values observed during the night are significant in the delay time, with which the wall—of remarkable thickness—releases the heat accumulated during the day, due to the exposure to sunlight. From data

reported in Figure 3b, an average value of the global heat transfer coefficient, around $0.65 \text{ W}/(\text{m}^2\text{K})$, was obtained. U was also calculated (Table 2) by applying ISO 6946 [33] to the stratigraphy of the wall, according to which, for an unventilated façade under steady-state conditions, it can be derived from Equation (2):

$$U = \frac{1}{R} = \frac{1}{\frac{1}{h_i} + \sum_{j=1}^n \frac{s_j}{\lambda_j} + \frac{1}{h_e}} \quad (2)$$

where R is the thermal resistance, s_j [m] and λ_j (W/(mK)) are the thickness and thermal conductivity of the j -th layer of the wall, n is the number of layers, h_i and h_e are the internal and external surface heat transfer coefficients, conventionally assumed to be 7.7 and $25.0 \text{ W}/(\text{m}^2\text{K})$.

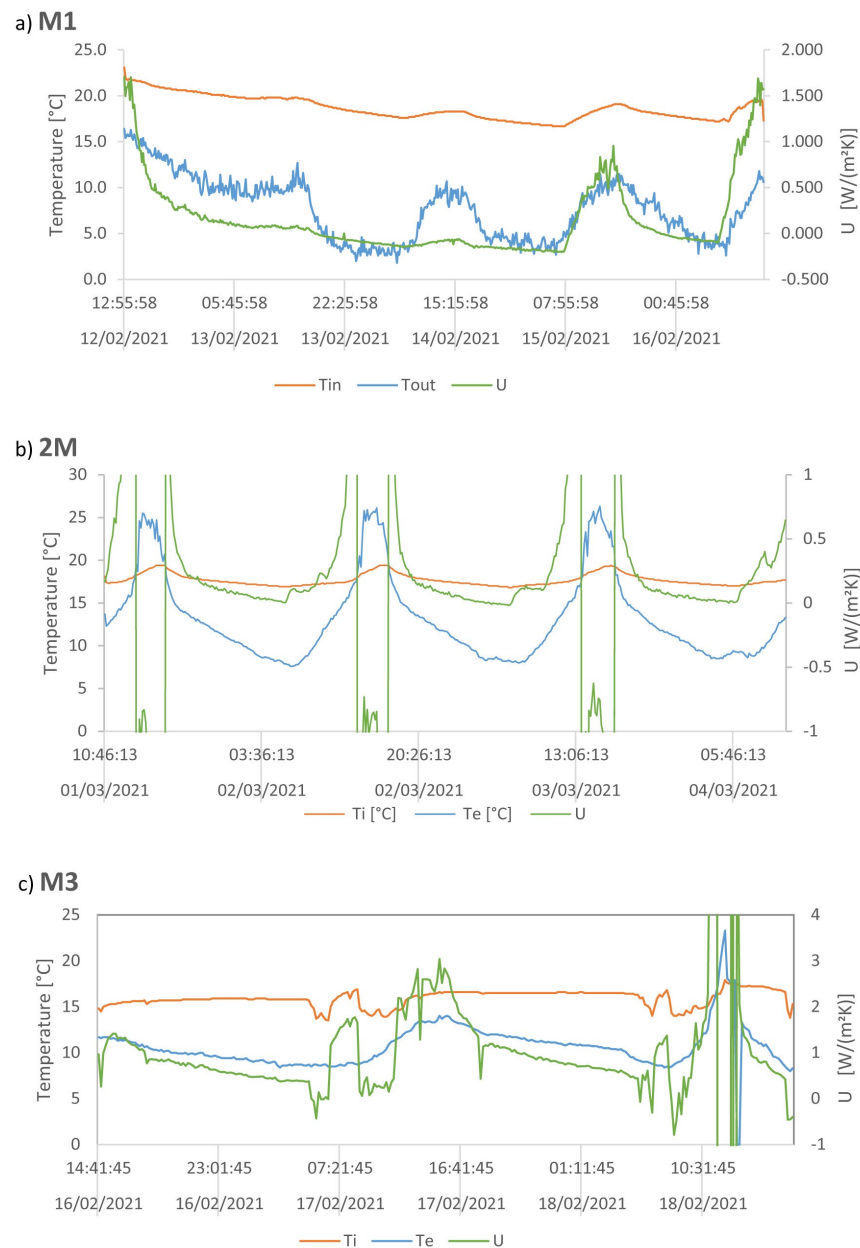


Figure 3. Temperature and heat flux measurements of the investigated façades: M1 (a), M2 (b), M3 (c).

The layers, in thickness and material, have been hypothesized through information on historical stratigraphies and direct observation of defects and lacks on the artifact, by naked eye and laser scanning. The estimated value was comparable with that measured and reported in the literature for similar wall elements [25]. It can be observed that the measured U is 8% higher than the average value calculated applying the standard [33] to the stratigraphy of the wall, equal to $0.55 \text{ W}/(\text{m}^2\text{K})$. The percentage difference between HFM and the theoretical values is less than 20%, which satisfies the ISO 9869–1 [32] criterion. The global heat transfer coefficient estimated for the opaque envelope (M1) of the building block object of the present study was about $0.58 \text{ W}/(\text{m}^2\text{K})$.

2.3. Dynamic Simulation Model

TRNSYS Software [34] was used for assessing the dynamic thermal behaviour and the energy performance for current and designed configuration conditions during a typical year. TRNSYS is a transient simulation program with a modular structure that considers the Transfer Function Method (TFM) and the main input data, which are: geometry and materials of the building, meteorological data, building internal gains, air infiltrations and ventilation rates.

2.3.1. Experimental Validation

The geometric 3D model of the building was implemented in TRNSYS by means of the Google SketchUp plug-in [35] and integrated with non-geometric information, managed by the TRNBuild interface through the multi-zone subroutine called Type 56 (Figure 4). The methodology included the subdivision of the building in thermal zones, taking into account the end uses (and expositions). In detail, five thermal zones were identified: the ground floor, the only one not heated (ZONE 0); the first floor (ZONE 1), which houses classrooms and offices; and the remaining three (ZONE 2, ZONE3, ZONE 4), consisting exclusively of offices. The North-Eastern wall, between the investigated wing and the main block of the building, was modelled as an adiabatic surface considering all of the two buildings at the same temperature: a boundary temperature input controlled by a custom equation was set. Other walls and floors were considered to be exchanging surfaces, where boundary conditions of the external walls and the roof were outside air conditions, whilst the lowest floor exchanged with the ground.

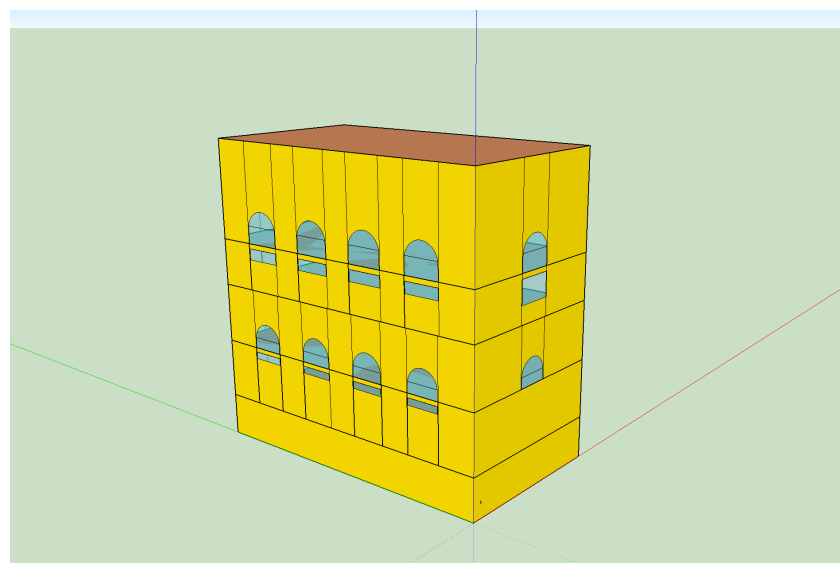


Figure 4. Model of the building.

Several previous works highlighted numerical problems in using the TFM with thick walls [26]. TRNSYS bases simulations on two different variables: time-step, which is the

time variable of the simulation, set in Simulation Studio; and time-base, the time series which characterizes the wall, set in TRNBuild. If the time-base from which the thick wall comes is too low, or the thick wall to be integrated is not associated to a correct choice of time-step, the software can lead to a miscalculation of the transfer function of the wall; this is caused by the wall model that considers the Z-transform. Walls which nearly reach the TRNSYS thickness limit (about 1.30 m), were cut into thinner walls, taking into account the maximum permissible thickness for each layer, which depends on the type of material [26]. After trials, a time-base of 4 h (greater than the default, which is equal to one hour) was used; indeed, in this case TRNBuild did not allow the calculation of the transfer function with a time-base less than or equal to 3 h. The STEP value in Simulation Studio must be bigger than the default (0.1), at least bigger than 0.5. The time-step used for the simulations was equal to 30 min.

TRNSYS allows the setting of the first indoor air temperature ($T_{i,0}$) and relative humidity (RH_0) values, which were considered for all the floors to be 23 °C and 50%, respectively, and corresponding to the start of the run period (t_0). Different initial temperatures caused the change of temperature-time trend, as observed by comparing the results obtained in $T_{i,0} = 23$ °C and $T_{i,0} = 20$ °C. The values achieved convergence after 3 days; therefore, to avoid the influence of the $T_{i,0}$ input, all of the simulations started 3 days before the first day of interest, including those for comparison with the experimental campaign.

The validation of the transient model was based on the indoor air temperatures measured on 12–16 February 2021 (Figure 5), using as input the outdoor air temperature registered during the same time period.

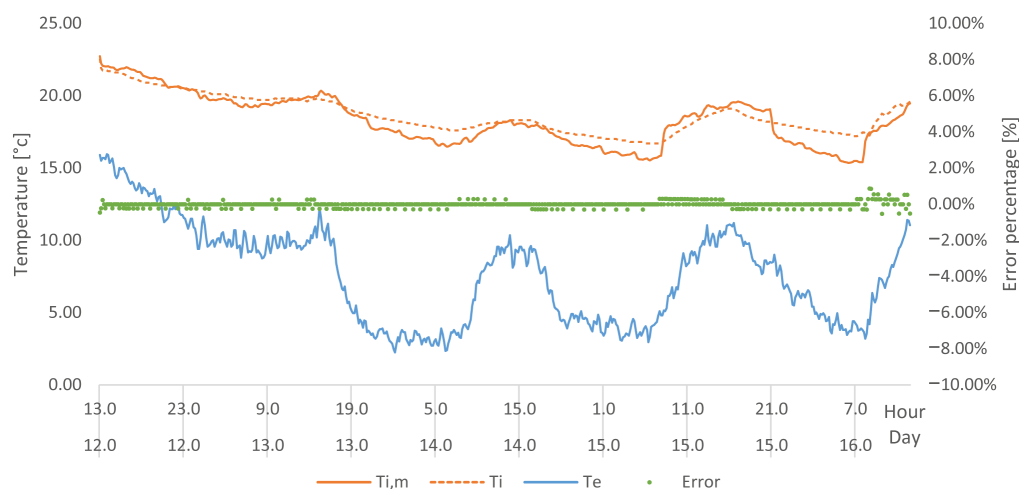


Figure 5. Experimental validation. Temperature profiles by measured data and TRNSYS simulations.

In modeling the infiltration and ventilation rates, internal gains associated with occupation, number of operating computers and lighting and thermal gains related to heating were considered, setting proper weekly schedules as the control strategy (Table 3). To create an appropriate gain type, heating loads for each floor were determined from information about the current HVAC system and then implemented in TRNBuild, split in radiative power and convective power equal to 20% and 80%, respectively.

Table 3. Model simulation hypotheses.

People	13 people—150 W/person * (floor 4) 12 people—150 W/person * (floor 2, floor 3) 48 people—150 W/person * (floor 1)	Working days from 8:00 a.m. to 8:00 p.m.
Devices	13 PCs with monitor—140 W/device (floor 4) 12 PCs with monitor—140 W/device (floor 2, floor 3) 48 PCs with monitor—140 W/device (floor 1)	Working days from 8:00 a.m. to 8:00 p.m.
Lighting	5 W/m ²	Working days from 8:00 a.m. to 8:00 p.m.
Heating and cooling systems operating periods		
Heating (20 °C) 01/11–15/04	Cooling (26 °C) 01/06–15/09	Working days from 7:00 a.m. to 8:00 p.m.
Infiltration rate		
	0.4 vol/h	Working days from 8:00 a.m. to 8:00 p.m.
Ventilation rate		
Classroom Office	0.6 vol/h (floor 1) 0.6 vol/h (floor 2, floor 3, floor 4)	Working days from 8:00 a.m. to 8:00 p.m.

* Heat gain rates from occupants, based on a 25.5 °C room at dry-bulb temperature. The value is adjusted on the basis of the normal percentage of men, women (gain equal to 85% of that for an adult male) and children (gain equal to 75% of that for an adult male) [36].

The following hypotheses were also assumed:

- The absorption coefficients were equal to 0.6 for the floor surface and 0.3 for the others [22];
- The wall external emissivity was equal to 0.9 [22];
- The convection coefficients were equal to 20 W/(m²K) for the external side and 5 W/(m²K) for the internal side, according to UNI EN ISO 6946 [33];
- The ground floor exchanged directly with the ground at 10 ± 5 °C [34], with the occurrence of the minimum surface temperature at the beginning of the calendar year.

Unless otherwise specified, the values refer to all floors. Internal gains from people and equipment were differentiated, other than by the size of the rooms, by destination. On floor 1, where together with the offices there are also classrooms, loads were referred respectively to 8 and 40 people, with their devices. As a heat source, people were considered “seating, light working, or typing”, contributing with 75 W to latent heat and 75 W to sensible heat, embracing the value assumed by TRNSYS [36] according to ISO 7730 [37]. Ventilation rates were determined as Air Changes Per Hour (ACPH, vol/h) from the surface of each floor and its prevalent actual use according to ASHRAE 62.1 [38], which requires for classrooms and offices an Area Outdoor Air Rate equal to 0.3 L/sm². Infiltration rates were identified according to the UNI EN 12207 [39], referring to the floor with the maximum glass surface, e.g., floor 4 (Table 1), and assuming that the windows belonged to Class 3. The amount of artificial light was calculated based on the mean Illuminance (E) for classrooms, $E = 300$ lux, and for laboratories and offices, $E = 500$ lux, in compliance with EN 12464 [40]; taking into account the floor area and a typical efficiency of the appliances equal to 80 lm/W. The closest of the default selectable values of TRNSYS Software was therefore adopted.

Calculated and measured data of indoor air temperatures are reported in Figure 5. The curves of the simulation are phase coincident with the experimental data. TRNSYS slightly overestimates the minimum temperatures, while the maximum are in good agreement with the measurements. The maximum difference between simulation and experimental data is about 2.75 °C. This discrepancy could be easily attributed to the experimental setup: measured values refer to local temperatures, whereas simulations give volume averaged results.

The weather data file intended to be used for the simulations was the Typical Meteorological Year (TMY) in the Meteororm files format (.TM2), specifically Roma-Ciampino, the

closest location to the building available in the TRNSYS database. It includes solar irradiance components (direct normal and global solar radiation on a horizontal plane), dry bulb temperature, relative humidity, wind velocity and direction. A preliminary comparison of outdoor air temperature (Figure 6) showed that experimental weather data were very different from the ones reported in the TMY meteorological file. In order to feed the model with more reliable data the Agenzia Regionale per lo Sviluppo e l'Innovazione dell'Agricoltura del Lazio (ARSIAL) [41] temperature database of the years 2020–2022 ($T_{e,ARSIAL}$) was taken into account. The data, with a frequency of 30 min, were averaged between three years and the values obtained were compared with those of the TRNSYS Meteonorm file, experiencing an average temperature increase by 4.1 °C during the summer months and by 2.1 °C during the winter months. The weather input file was modified accordingly.

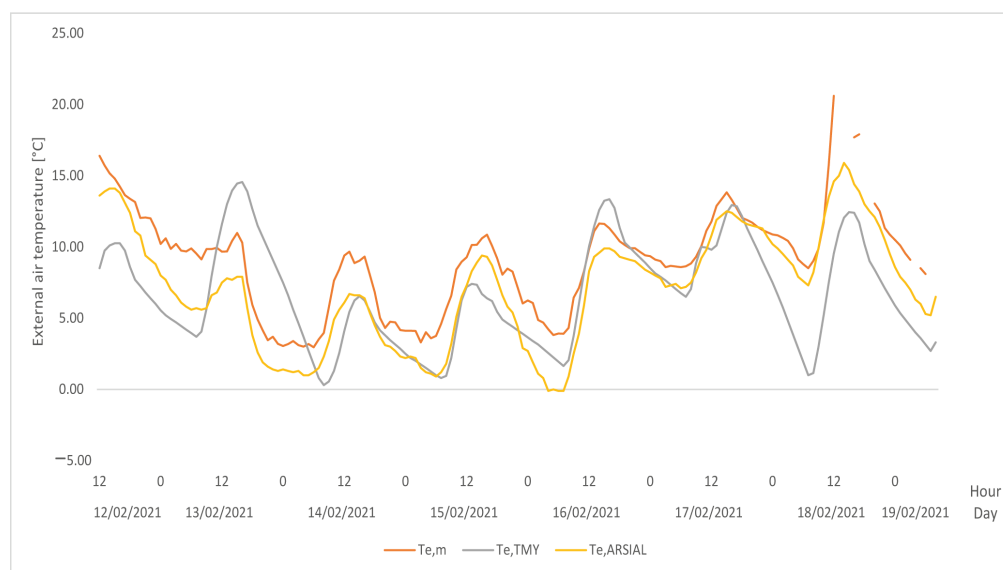


Figure 6. Outdoor air temperature: difference between original Meteonorm file, ARSIAL weather database and measurements.

2.3.2. Numerical Analysis

The validated model was used to evaluate the current scenario and to compare it with several passive solutions, with the aim of improving energetic performance and thermal comfort of the building by means of proposals that can be adopted in similar situations with constrained Architectural Heritage.

In order to assess the annual energy demand of the building, the desired temperature conditions were set for each floor, except for the ground floor: the room air temperature setpoint was equal to 20 °C for the heating period and 26 °C for the cooling period, 1 November–15 April and 1 May–15 September respectively, as stated for the D climatic zone [42]. The operation of the HVAC system was set on the basis of the occupants' presence, following a schedule which required the system being turned on from 8:00 a.m. to 08.00 p.m. in the workdays (max 12 h heating as per regulation [42]) and turned off during the weekend. Humidification and dehumidification were not taken into account. Moreover, in order to evaluate the annual energy consumption, the ventilation rate was not considered when the HVAC system was turned on. Gains were the same as those used for validation (Table 3), whereas, unlike the previous case, air conditioning system was not considered as an input gain, but configured as described just above.

For the evaluation of the thermal behavior of the glazings, indoor thermal conditions and thermal comfort, no HVAC system was considered in the simulation model. Additionally, in this case, gains and assumptions were those listed in Table 3.

The influence of three different solutions for the transparent surfaces on indoor environmental conditions and occupant thermal comfort was investigated. The results were

compared with the current glazing system, constituted by a single 4 mm glass pane (SGU). In particular, the replacement with Double Glazing Units (DGUs) with low-e or sunlight control glass panes was considered. Beside this, one of the examined cases was the threshold-driven internal shading activation. The blinds are closed completely if a threshold is exceeded: more than 150 W/m^2 on the outside vertical façade. On the other hand, the blinds will be retracted when the irradiation on the outside vertical façade falls below that threshold [20]. The above-mentioned strategy, although it is the most conservative, is therefore most easily achievable and needs to be compared with the window substitution strategies in terms of energy demand for the electric lighting. The reason for this is that the daylight autonomy needs to be implemented with artificial lighting in order to respect the minimum requirements during office hours [20], e.g., here 500 lux.

The assessed scenarios are summarized below, where the lowercase letter followed by Roman numeral represents the scenario's ID: the letter "a" or "p" is to specify whether it is an ante operam or post operam case; the number identifies the glazing type. The respective glazing system properties, alongside the corresponding glass and assembly details, are explained in Table 4.

- a.I.: SGU float glass (currently employed);
- p.II: SGU float glass coupled with internal shading;
- p.III: DGU sunlight control glass;
- p.IV: DGU low-e glass.

Table 4. Glazing system properties (from TRNBuild database [36]).

ID Scenario	Glazing	Characteristics	τ_{vis} [-]	ρ_{sol} [-]	SHGC [-]	U [W/(m ² K)]	TRN Code *
a.I	4	Float glass	0.901	0.075	0.855	5.68	1101
p.III	6/16/6	Float and sunlight control glasses with argon (90%) in the interspace	0.659	0.218	0.333	1.29	3004
p.IV	4/16/4	Float and low-e glass with argon (90%) in the interspace	0.713	0.311	0.533	0.98	12005
p.II	4	Float glass+ shading	0.901	0.075	0.855	5.68	1101

* TRN code is the identification code in TRNSYS Software.

The glazing system used for the p.III scenario is characterized by a low Solar Heat Gain Coefficient (SHGC), equal to 0.333. The one used for the p.IV scenario features instead a low-e treatment, consisting of a coating on the third surface from the outer to the inner layer, responsible for a global heat transfer coefficient value of $0.98 \text{ W/(m}^2\text{K)}$.

For the evaluation of PMV and PPD thermal comfort indices, a comfort type was created, which considers for the whole year a metabolic rate of $M = 1.2$ met, and relative air velocity equal to 0.1 m/s ; additionally, it has a clothing factor set by an input file in Simulation Studio that provides $I_{cl} = 1.5$ clo from December to May and $I_{cl} = 0.5$ clo in the remaining months, both for men and women. The Mean Radiant Temperature was determined by the TRNBuild internal calculator, based on area-weighted mean surface temperatures.

3. Results

3.1. Energy Performance Results

The monthly energy consumption can be deduced for each heated/cooled floor from Figure 7.

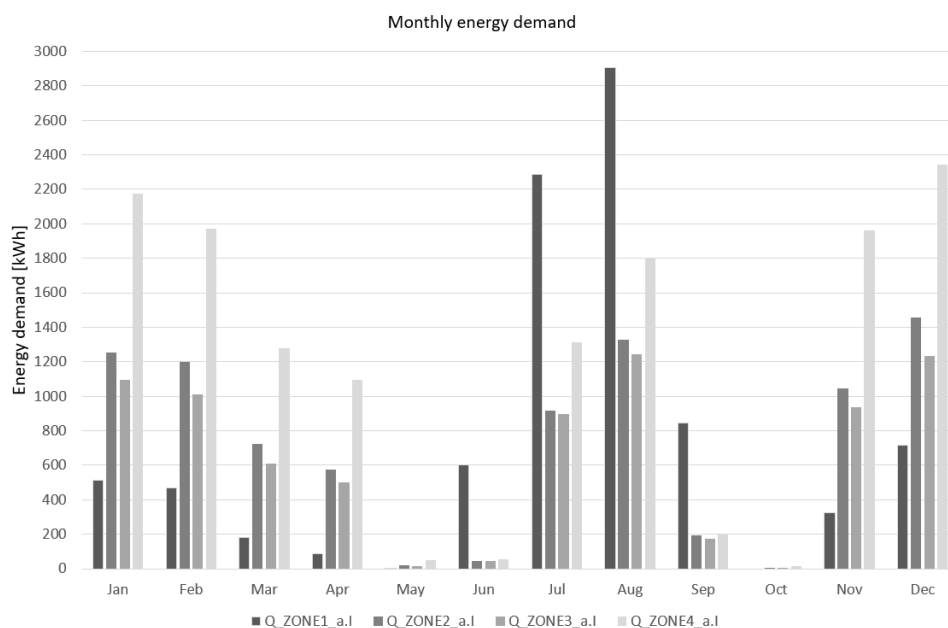


Figure 7. Monthly energy demand: comparison between thermal performance of different floors in current configuration.

The winter energy demand increases noticeably for the fourth floor (average value around 1805 kWh), as it has a higher number of surfaces dispersing to the outside, and a greater percentage of glazing than the other floors (Table 1). Summer loads are considerable for floor 1, because of the higher occupancy index; hosting rooms for university classrooms, it has a standard presence of 48 people with as many devices, that both contribute to internal loads against about 12 people on the other floors. The overall maximum energy demand for this configuration is in August and is equal to 2907 kWh. The occupancy is also responsible for the fact that for the same glass area and with a floor in contact with an unheated room, floor 1 has a winter energy demand equal to 0.43 times that of floor 3. For the same number of occupants, floor 2, with a larger window area than floor 3 (+62%), has a heating requirement of 6272 kWh against 5410 kWh, while the energy demands during the cooling period are comparable (2480 kWh and 2356 kWh, respectively).

Currently, at the level of the entire building (Table 5), the unfavorable situation is the winter one, with 24,869 kWh against the 14,847 kWh of the summer period. The most efficient solution is represented by the use of low-e glass (scenario IV), which offers an improvement in heating by 15% and cooling by 12%. This result is in line with the trend observed for even more recent buildings [22]. The option of introducing solar shading offers a good performance in summer, reducing the energy demand by 19%.

Table 5. Summer, winter and overall annual energy demand.

	a.I	p.II	p.III	p.IV
TOTAL Summer [kWh]	14,847.10	11,961.83	11,104.07	13,099.10
TOTAL Winter [kWh]	24,869.16	29,456.64	24,793.91	21,219.84
TOTAL Overall [kWh]	39,716.25	41,418.47	35,897.98	34,318.95

It was decided to further investigate the second floor, as it was representative for the use prevalent in the building (offices) and significant in terms of the glazed to opaque surface ratio, which is of central interest in this work. The most onerous situation is confirmed to be the winter season (Figure 8). By means of TRNSYS Software, ante and low-e (p.IV) assessment showed an overall annual reduction of 17%, decreasing from 8752 kWh/year to 7304 kWh/year, as reported in Figure 8. This optimization brings the greatest benefits in

winter, while in summer it is overcome by the use of solar control glazings, which offer a further reduction of 17%. The drawback of sunlight control systems is a winter behavior similar to that of current windows, particularly throughout the temperate months. Without the need to replace the glass, it is possible to achieve a summer performance similar to that of low-e systems, obtaining even better results, with the introduction of shading elements. Shading reduces the monthly cooling demand compared to the current case to up to more than 25%. Maintaining the shading control linked to the radiation amount incident on the wall, even in winter is noted, for the floor under consideration, an increase of 1028 kWh compared to the situation with single float glass, significant of how the treatment of visual discomfort could adversely affect seasonal consumption. In the specific situation of the investigated floor, the aforementioned increase is more contained than what is seen for the entire building, being limited to 16% (vs. 18%).

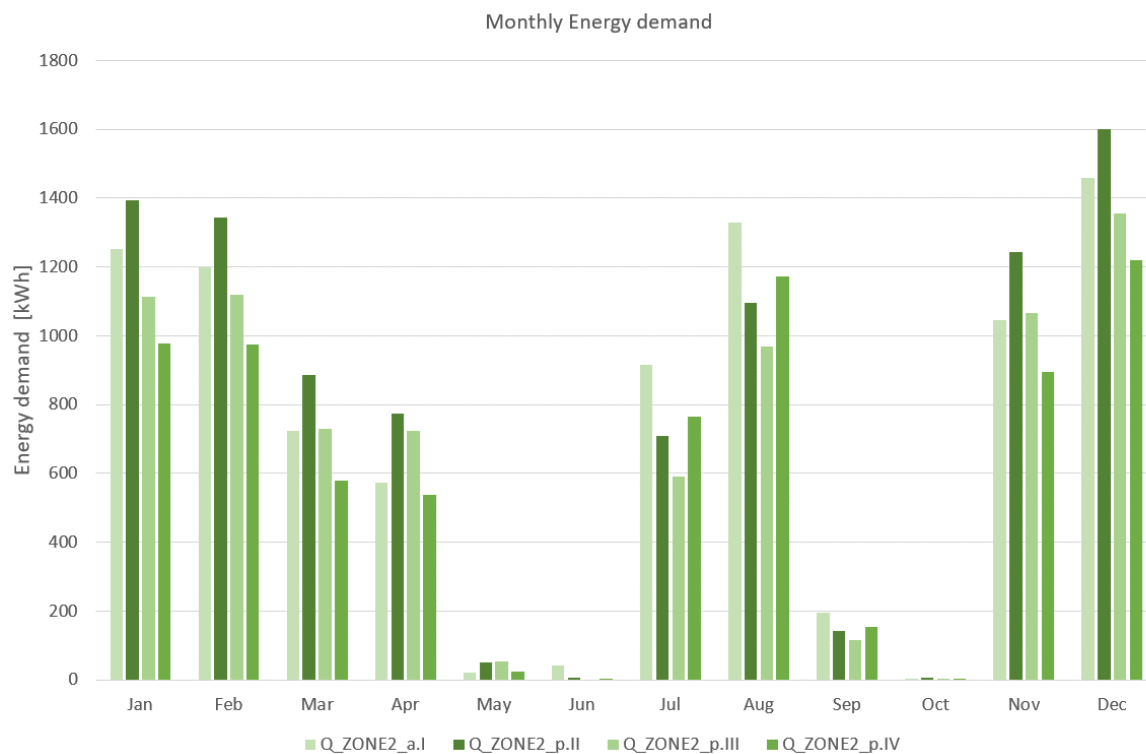


Figure 8. Monthly energy demand: comparison between thermal performance in current and optimized configurations for a typical inner floor with high transparent percentage (floor 2).

In Figure 9, the annual distribution of thermal loads for the current state and for the designed configuration with low-e windows were compared. This took into account a guaranteed room air temperature during working hours equal to 20 °C in winter and 26 °C in summer, based on occupancy and other internal gains and boundary conditions such as infiltration (see Section 2.3.1). The average maximum power drops in the heating season were from 12.4 kW to 11.0 kW, and in the cooling season from 6.3 kW to 5 kW.

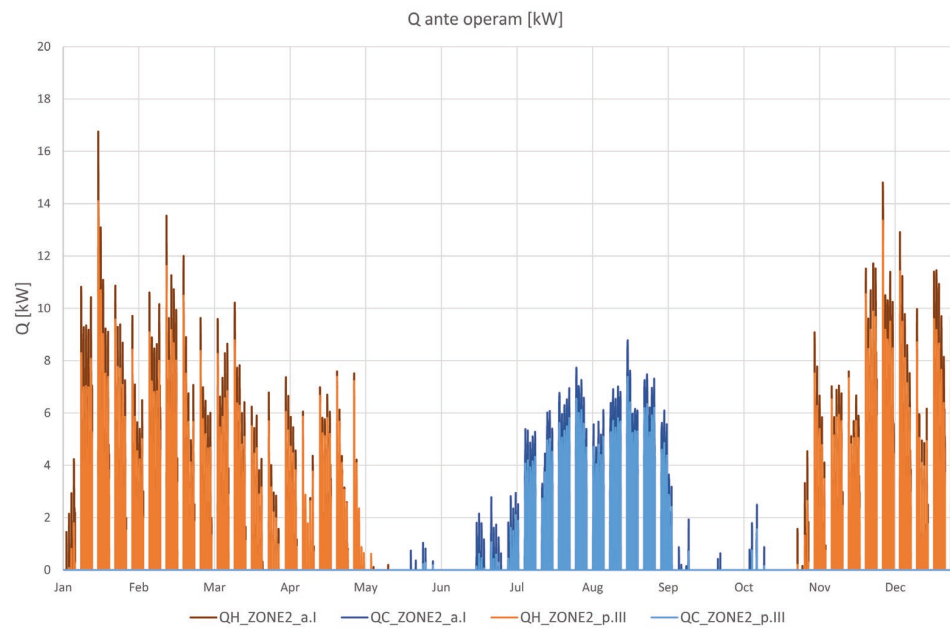


Figure 9. Annual distribution of instantaneous power: current and designed configuration p.IV (floor 2).

3.2. Temperature and Comfort

Floor 2 was analyzed further, delving into ambient and surface temperatures and the comfort of the occupants. The temperature trends during a typical week in winter and summer, of the inner surface of the single glass currently adopted, are displayed in Figures 10 and 11. The maximum radiation is reached in summer on the surface of the South-oriented glass surface (dotted green line), but corresponds to a time of the day in which the external air temperature is low. The maximum peak of surface temperature occurs for the West surface (solid blue line), because there the radiation is maximum at the same time as the maximum temperature of the external air.

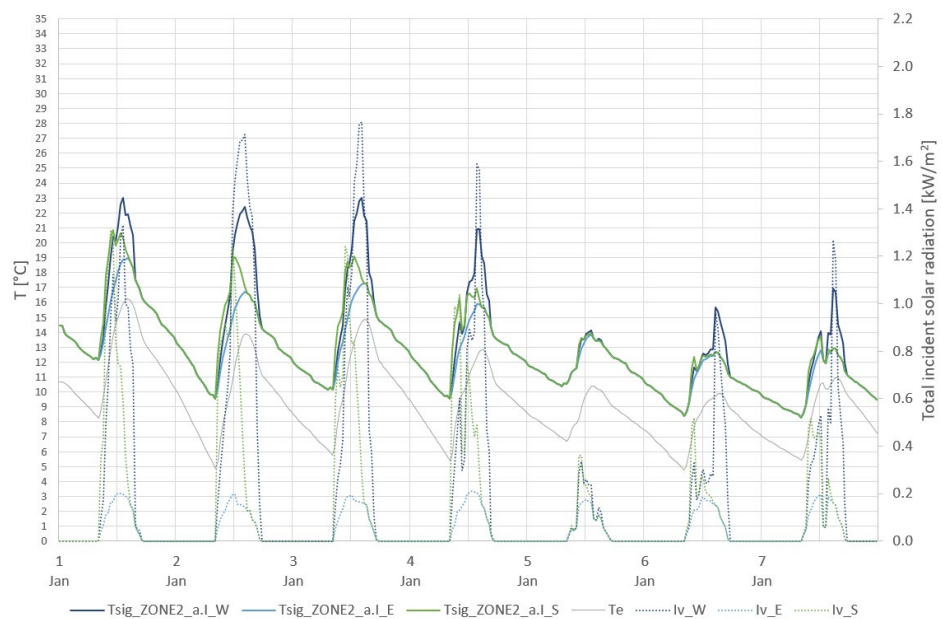


Figure 10. Internal surface temperature of current glazing system for different orientations; winter period: January, first week (floor 2).

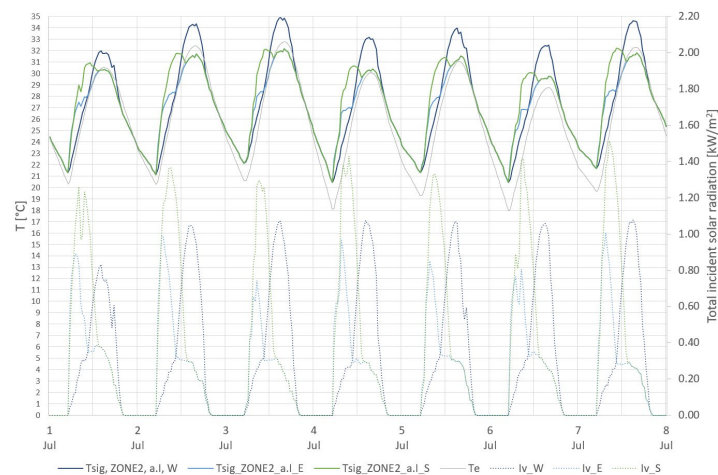


Figure 11. Internal surface temperature of current glazing system for different orientations; summer period: July, first week (floor 2).

Figure 12 compares the different solutions proposed in the winter season, and refers to windows facing North-West. Changing the type of glass, with the introduction of double-glazings, we immediately found the ability to maintain a higher internal surface temperature; the increases are of about 8 °C, emphasized in the hours between 8.00 and 16.00, in which the contribution of solar radiation takes place. In this case, the low emission treatment enhances the benefits of the double glass, allowing to reach up to 11 °C more than the temperature you would have on the inside of the single glass of the current window. The fact that the use of this type of glass is particularly indicated in situations where the solar contribution is substantial is evident in days such as the fifth of Figure 12, where for a day with solar radiation incident less than 0.042 kW/m² the difference between DGU low-e and with solar control is about 1 °C. The external surface temperature of the two proposed glass alternatives is exactly overlapping with the profile of the external air temperature, and the deviations occur when there is also solar radiation. In general, therefore, in the winter season between the internal and external surface of a double glass, there is a temperature difference of 10 °C, while for the single panel there were similar values between the two sides (Figure 10).

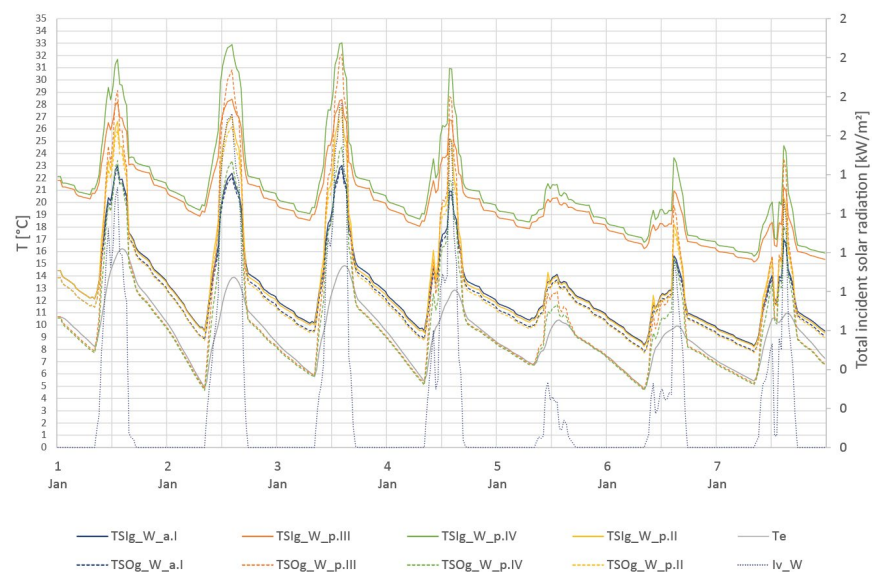


Figure 12. Surface temperature for different glazing systems North-West oriented; winter period: January, first week (floor 2).

In winter, the indoor temperature trend (not considering HVAC systems) keeps very far from the setpoint (Figure 13) in a constant way over time, unlike that in the summer period (Figure 14) which is extremely high and limited to shorter time periods; this is one of the reasons why thermal loads are remarkable for the heating period. In winter (Figure 13), the current glazing and the solar control DGU (III) are comparable. Instead, during the night the mean air temperature obtained with solar control DGU (III) is higher than that of the existing glazing because of the lower global heat transfer coefficient value ($1.3 \text{ W}/(\text{m}^2\text{K})$). DGU IV raises the temperature in comparison with SGU by about $1 \text{ }^\circ\text{C}$. Glazing IV allows the best peak temperature control during the morning. Existing glazing and shading do not allow a very good control of the indoor air temperature, which drops below $13 \text{ }^\circ\text{C}$ during the coldest hours.

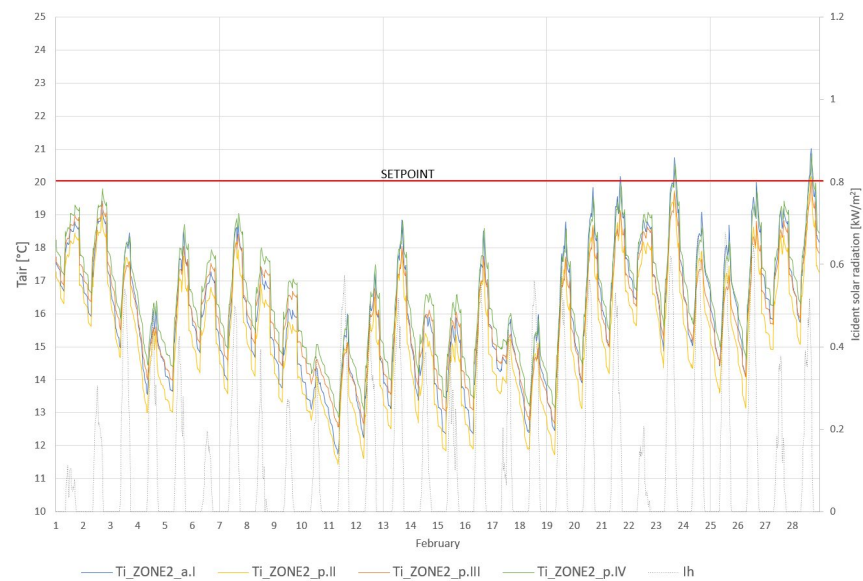


Figure 13. Effects of glazing systems on mean indoor air temperature; winter period: February (floor 2).

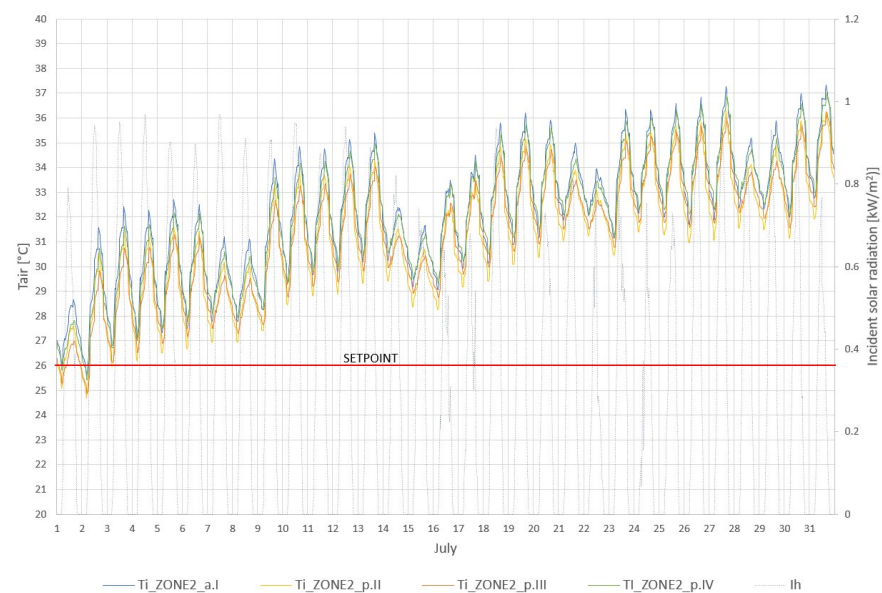


Figure 14. Effects of glazing system on mean indoor air temperature; summer period: July (floor 2).

In summer (Figure 14) all the proposed solutions for the windows ensure better temperature control, decreasing the morning peaks by at least $0.5 \text{ }^\circ\text{C}$. The behavior during the coolest hours with glasses I and IV is comparable, because of the lower thermal global

heat transfer coefficient value of type IV ($U = 0.98 \text{ W}/(\text{m}^2\text{K})$); the daytime improvement is particularly noticeable on days in which the radiation is higher, thanks to the low SHGC (0.533 vs. 0.855) of the low-e DGU under consideration. The fact that solar control is the best solution for the cooling period is evident from the trends reported for the month of July: the mean temperature from the current case to III is lowered by $0.6 \text{ }^\circ\text{C}$. This can be attributed to a SHGC equal to 0.333. Shading decreases all temperature extremes of the current configuration by about $1 \text{ }^\circ\text{C}$, with a daily ΔT higher than that of other solutions. This particularly significant mitigation during daytime peak hours makes this configuration not distant in performance from DGU with low-e. The use of shading is the most outperforming configuration in the evening hours; although they represent an additional obstacle to the passage of heat between the inside and outside, they do not significantly reduce the high global heat transfer coefficient of the single glass currently used ($U = 5.68 \text{ W}/(\text{m}^2\text{K})$).

While evaluating PMV during the occupancy period (8.00 a.m. to 8.00 p.m.) in the current scenario, it can be noted that in winter the discomfort (in relation to PMV values on the negative half-axis as expected) is lower than in the hot months (Figures 15 and 16). The mean PMV is -0.54 , light cold, whereas in summer it stands around 2.03, warm. The daily winter PMV variation is equal to 0.6 (between -0.31 and -0.95), lower than that of summer, $\Delta = 0.7$ (between 1.65 and 2.33). Both in summer and in winter, referring to working hours, the greater improvement obtainable by employing glazing systems with a low-e treated pane (scenario p.IV) happens at the maximum discomfort time, which in the former case occurs at 8.00 a.m., and in the latter at 4:30 p.m. During the cold season (Figure 15) the low-e DGU enhances the worst registered PMV, bringing it to -0.81 ; this raises it to about 0.14 points. In summer, the greatest discomfort is not due to the maximum temperature of the external air, as seen in the first day reported in Figure 16 ($\text{PMV} = 1.98$), but is more affected by solar radiation, as shown in the same Figure 16 for the last simulated days ($\text{PMV} = 2.29$). This shows a significant need to intervene at the level of transparent elements to improve the performance of the building for the occupants. During the hot season, the lowering of the maximum indoor air temperature of floor 2 by the low-e DGU by $0.56 \text{ }^\circ\text{C}$ corresponds to a reduction in the sensation of heat by 0.18 points (day 1 in Figure 16), passing from the feeling of warm to slightly warm. During the cool hours, the difference from the SGU case is limited by the reflective effect of the glazed surface in IR wavelengths; the same phenomenon causes the increase of the PMV from 1.12 to 1.23 during the evening hours of days in the presence of high solar radiation.

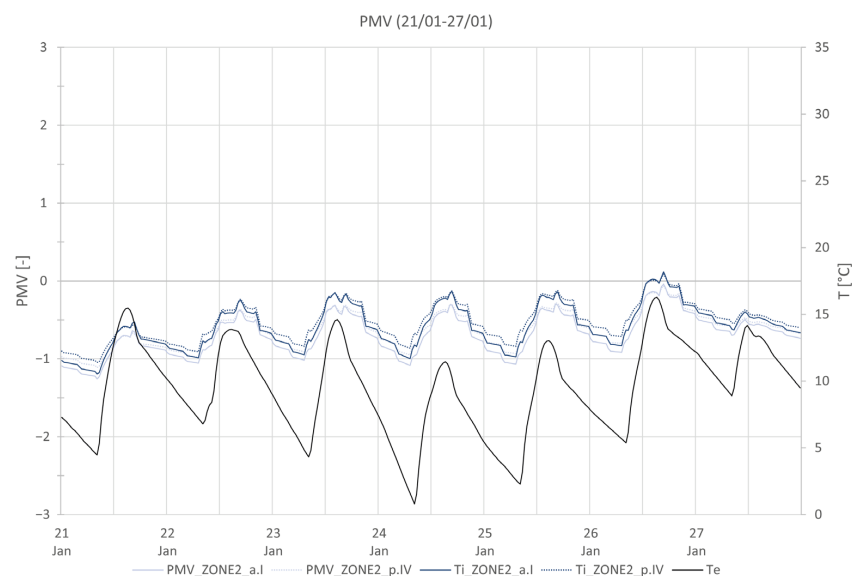


Figure 15. Comparison between PMV in current and low-e configuration during a typical winter week (floor 2).

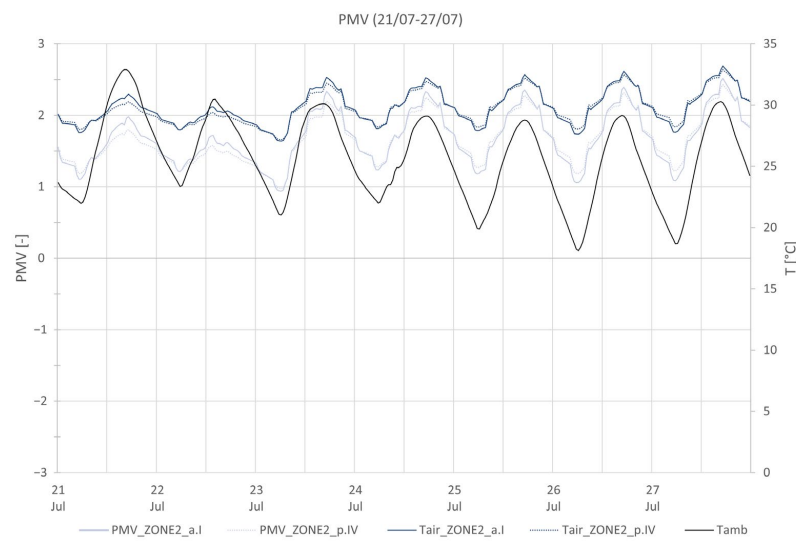


Figure 16. Comparison between PMV in current and low-e configuration during a typical summer week (floor 2).

During a typical day in the summer (Figure 17), the PPD with a SGU varies from 82% to 20%, corresponding to a PMV of 2.14, warm, and 0.83, light warm, respectively; the lower peaks are only qualitatively indicative, since the occupation period does not include the time period from 8.00 p.m. to 8.00 a.m. The abovementioned values refer to the trend of the fourth floor, which undergo the greatest oscillation due to the greater area of external dispersant surfaces compared to the other floors. PPD fluctuation is reduced as you move to the lower floors: at the first floor, the minimum PPD of 32% has a significant ground contribution. In the mid-season period (May), PPD during working hours is between 95% for the early hours of the day and 50% around 3 p.m., in compliance with outdoor air temperature values, about 12 °C and 21 °C respectively; this is unlike what is seen for July (Figure 17) when the mean external temperature is approximately 30 °C. By employing low-e glasses the highest peaks are reduced up to 12.5%, with the maximum benefit found for floor 4. The dissatisfied percentage increase during cold hours is slight: PPD becomes 23% ($\Delta = +3$ percentage units).

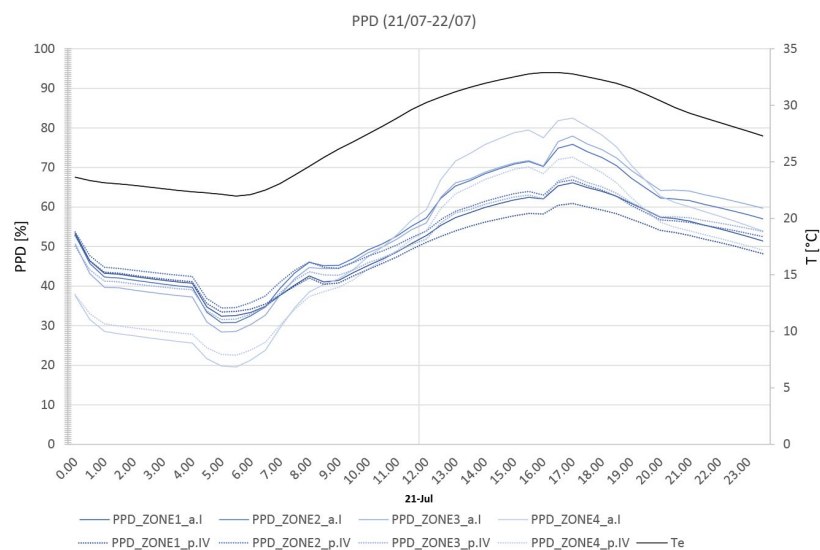


Figure 17. Comparison between PPD in current and low-e configuration of different floors during a typical summer week.

4. Conclusions

In the last decade, the issue of energy efficiency has become increasingly important, taking a prominent role in the development goals of countries. Given that buildings have a high share in total energy consumption, it is crucial to improve their energy performance both in environmental and economic terms. Although efforts are involved in enhancing new buildings, existing buildings are especially attractive, as proved by the publication of several guidelines for their improvement. They represent an interesting topic mainly due to the consistency of the stock on the Italian area, which is equal to 30% of the total amount of the built environment; and to the need to balance energy efficiency improvement with the requirements of preservation. When facing constructions of historical value, between major constraints occurs the impossibility of modifying the façade. Working on the substitution of the current windows allows us to achieve promising results, while maintaining a low visual impact of the intervention.

The seat of the Engineering Faculty of Sapienza University of Rome, belonging to cultural heritage and characterized by a quite high Window-to-Wall Ratio, was selected in the present study with the aim of defining the most suitable solutions for fenestration for public buildings of the XVIII century located in warm climate areas. High performance glazing solutions, together with the introduction of shading systems as “not-destructive” options to reduce overheating (which may occur especially during the hot season) were proposed and assessed, quantifying their direct impact on the indoor temperature, energy consumption and occupants’ comfort (PMV and PPD).

For this purpose, a dynamic simulation model in TRNSYS was validated by data from the on-site monitoring campaign for wall characterization.

A useful tool for historical buildings was therefore provided, which enabled us to hypothesize different technological solutions and HVAC systems for controlling the indoor thermo-hygrometric conditions, and to evaluate their effects on energy performance and thermal comfort, individuating the most appropriate design option and giving recommendations for a specific building category.

The main results are summarized as follows:

- The software limitation in understanding thick and inertial walls was fixed by dividing walls with thickness near to the TRNSYS limit (about 1.30 m) in thinner layers, considering that each layer has a maximum permissible thickness, which depends on the material’s type (0.5 m for bricks).
- Since the cooling and heating demand are strongly affected by the external climate conditions, a Meteonorm weather file correction was performed to make it more representative of the real climatic conditions. It was based on data gathered during the experimental campaign and ARSIAL Society climatic database, and allowed us to better compare the simulation results and the experimental data, and to validate the model.
- Configuration IV offers savings of up to 5397 kWh/year for the seat; shading also offers good results for the summer period, leading to a reduction of 2285 kWh in the energy demand.
- Existing glazing and shading do not allow for good control of the indoor air temperature, which drops below 13 °C during the coldest hours in winter. All proposed solutions for the windows ensure better temperature control during summer, decreasing the morning peaks by at least 0.5 °C.
- The substitution of the current SGU with low-e DGU in the summer season results in a PPD reduction of up to 72% for floor 4 ($\Delta = -10$ percentage units, maximum reduction), with proportional advantages to the number of dispersant surfaces. The dissatisfied percentage during cool hours is similar to that of ante operam configuration, increasing only by 3 percentage units.

Author Contributions: A.V.: Conceptualization, Methodology, Writing—Reviewing and Editing, Supervision, Project Administration. M.D.M.: Investigation, Data Curation, Writing—Original Draft Preparation, Writing—Reviewing and Editing. C.V.F.: Investigation, Data Curation, Software, Validation, Formal Analysis, Writing—Original Draft Preparation, Writing—Reviewing and Editing, Visualization. All authors have read and agreed to the published version of the manuscript.

Funding: This research received no external funding.

Institutional Review Board Statement: Not applicable.

Informed Consent Statement: Not applicable.

Data Availability Statement: Not applicable.

Conflicts of Interest: The authors declare no conflict of interest.

Nomenclature

Abbreviations

ARSIAL	Agenzia Regionale per lo Sviluppo e l’Innovazione dell’Agricoltura del Lazio
BSP	Building Simulation Programs
DGU	Double Glazing Unit
DRF	Direct Root Finding
GCHP	Ground Coupled Heat Pump
GHG	Greenhouse Gases
HFM	Heat Flow Meter
HP	Heat Pump
LC	Life Cycle
M1	First measuring point
M2	Second measuring point
M3	Third measuring point
SGU	Single Glazing Unit
SCF	Solar Control Film
TFM	Transfer Function Method
TMY	Typical Meteorological Year
a	Scenario ante operam
p	Scenario post operam
Roman numeral(I-IV)	Glazing type

Symbols

ACPH	Air Changes Per Hour	[vol/h]
E	Mean illuminance	[lux]
h_e	External surface heat transfer coefficient	[W/(m ² K)]
h_i	Internal surface heat transfer coefficient	[W/(m ² K)]
I_h	Total horizontal incident radiation	[kW/m ²]
I_v	Total vertical incident radiation	[kW/m ²]
PMV	Predicted Mean Vote	[-]
PPD	Predicted Percentage of Dissatisfied	[-]
q_m	Measured heat flux	[W/m ²]
Q	Thermal energy	[kWh]
Q_C	Thermal energy for cooling	[kWh]
Q_H	Thermal energy for heating	[kWh]
R	Thermal resistance	[(m ² K)/W]
RH	Relative humidity	[%]
RH_0	First relative humidity ($t = t_0$)	[%]
s	Thickness	[m]
SHGC	Solar Heat Gain Coefficient	[-]
t	Time	[h]
t_0	Start time	[h]

$T_{e,ARSIAL}$	External air temperature from ARSIAL	[°C]
$T_{e,TMY}$	External air temperature from TMY	[°C]
$T_{e,m}$	Measured external air temperature	[°C]
T_e	External air temperature	[°C]
$T_{i,0}$	First indoor air temperature ($t = t_0$)	[°C]
$T_{i,m}$	Measured indoor air temperature	[°C]
T_i	Simulated indoor air temperature	[°C]
T_{seg}	External surface temperature of the glass	[°C]
T_{sig}	Internal surface temperature of the glass	[°C]
U	Global heat transfer coefficient	[W/(m ² K)]
WWR	Window-to-Wall Ratio	[%]
WWRs	Specific Window-to-Wall Ratio	[%]
λ	Thermal conductivity	[W/(mK)]
ρ_{sol}	Solar reflectance	[-]
τ_{vis}	Visible transmittance	[-]
<i>Subscripts</i>		
C	heating	
e	external	
g	glass	
h	horizontal	
H	cooling	
i	indoor	
j	index for j-th value/element	
m	measured	
s	simulated	
se	external surface	
si	internal surface	
sol	solar	
v	vertical	
vis	visible	
$_ZONE_x$	thermal zone “x”	
0	first value ($t = t_0$)	

References

1. IEA (International Energy Agency). *World Energy Outlook*; IEA: Paris, France, 2012.
2. IAE. Energy Efficiency Indicators Highlights. 2016. Available online: <https://www.oecd.org/publications/energy-efficiency-indicators-9789264268692-en.htm> (accessed on 14 July 2022).
3. Ozbalta, T.G.; Yildiz, Y.; Bayram, I.; Yilmaz, O.C. Energy performance analysis of a historical building using cost-optimal assessment. *Energy Build.* **2021**, *250*, 111301. [[CrossRef](#)]
4. Mauri, L.; Vallati, A.; Ocloń, P. Low impact energy saving strategies for individual heating systems in a modern residential building: A case study in Rome. *J. Clean. Prod.* **2019**, *214*, 791–802. [[CrossRef](#)]
5. Pacchiega, C.; Fausti, P. A study on the energy performance of a ground source heat pump utilized in the refurbishment of an historical building: Comparison of different design options. *Energy Procedia* **2017**, *133*, 349–357. [[CrossRef](#)]
6. Emmi, G.; Zarrella, A.; De Carli, M.; Moretto, S.; Galgaro, A.; Cultrera, M.; Di Tuccio, M.; Bernardi, A. Ground source heat pump system in historical buildings: Two Italian case studies. *Energy Procedia* **2017**, *133*, 183–194. [[CrossRef](#)]
7. Gomes, M.G.; Rodrigues, A.M.; Natividade, F. Thermal and energy performance of medical offices of a heritage hospital building. *J. Build. Eng.* **2021**, *40*, 102349. [[CrossRef](#)]
8. Qu, K.; Chen, X.; Wang, Y.; Calautit, J.; Riffat, S.; Cui, X. Comprehensive energy, economic and thermal comfort assessments for the passive energy retrofit of historical buildings—A case study of a late nineteenth-century Victorian house renovation in the UK. *Energy* **2020**, *220*, 119646. [[CrossRef](#)]
9. Tiberi, M.; Carbonara, E. Comparing Energy Improvements and Financial Costs of Retrofitting Interventions in a Historical Building. *Energy Procedia* **2016**, *101*, 995–1001. [[CrossRef](#)]
10. Silvero, F.; Montelpare, S.; Rodrigues, F.; Spacone, E.; Varum, H. Energy retrofit solutions for heritage buildings located in hot-humid climates. *Procedia Struct. Integr.* **2018**, *11*, 52–59. [[CrossRef](#)]
11. Jain, A.S.; Saikia, P.; Rakshit, D. Thermal energy performance of an academic building with sustainable probing and optimization with evolutionary algorithm. *Therm. Sci. Eng. Prog.* **2020**, *17*, 100374. [[CrossRef](#)]
12. Bastien, D.; Athienitis, A.K. Methodology for selecting fenestration systems in heating dominated climates. *Appl. Energy* **2015**, *154*, 1004–1019. [[CrossRef](#)]

13. Jelle, B.P.; Hynd, A.; Gustavsen, A.; Arasteh, D.; Goudey, H.; Hart, R. Fenestration of today and tomorrow: A state-of-the-art review and future research opportunities. *Sol. Energy Mater. Sol. Cells* **2012**, *96*, 1–28. [[CrossRef](#)]
14. Grynning, S.; Gustavsen, A.; Time, B.; Jelle, B.P. Windows in the buildings of tomorrow: Energy losers or energy gainers? *Energy Build.* **2013**, *61*, 185–192. [[CrossRef](#)]
15. Pereira, J.; Gomes, M.G.; Rodrigues, A.M.; Almeida, M. Thermal, luminous and energy performance of solar control films in single-glazed windows: Use of energy performance criteria to support decision making. *Energy Build.* **2019**, *198*, 431–443. [[CrossRef](#)]
16. Litti, G.; Audenaert, A.; Lavagna, M. Life cycle operating energy saving from windows retrofitting in heritage buildings accounting for technical performance decay. *J. Build. Eng.* **2018**, *17*, 135–153. [[CrossRef](#)]
17. Figueroa-Lopez, A.; Arias, A.; Oregi, X.; Rodríguez, I. Evaluation of passive strategies, natural ventilation and shading systems, to reduce overheating risk in a passive house tower in the north of Spain during the warm season. *J. Build. Eng.* **2021**, *43*, 102607. [[CrossRef](#)]
18. Tzempelikos, A.; Bessoudo, M.; Athienitis, A.K.; Zmeureanu, R. Indoor thermal environmental conditions near glazed facades with shading devices e Part II: Thermal comfort simulation and impact of glazing and shading properties. *Build. Environ.* **2010**, *45*, 2517–2525. [[CrossRef](#)]
19. Freewan, A.A.Y. Impact of external shading devices on thermal and daylighting performance of offices in hot climate regions, *Sol. Energy* **2014**, *102*, 14–30.
20. Wienold, J. Dynamic simulation of blind control strategies for visual comfort and energy balance analysis. In Proceedings of the 10th IBPSA Conference: Building Simulation, Beijing, China, 3–6 September 2007; pp. 1197–1204.
21. Xie, J.; Omidfar, S.A. Simulation-assisted data-driven method for glare control with automated shading systems in office buildings. *Build. Environ.* **2021**, *196*, 107801. [[CrossRef](#)]
22. Buratti, C.; Moretti, E.; Belloni, E.; Cotana, F. Unsteady simulation of energy performance and thermal comfort in non-residential buildings. *Build. Environ.* **2013**, *59*, 482–491. [[CrossRef](#)]
23. Vallati, A.; Mauri, L.; Colucci, C. Impact of shortwave multiple reflections in an urban street canyon on building thermal energy demands. *Energy Build.* **2018**, *174*, 77–84. [[CrossRef](#)]
24. Vallati, A.; Grignaffini, S.; Romagna, M.; Mauri, L.; Colucci, C. Influence of Street Canyon’s Microclimate on the Energy demand for space cooling and heating of buildings. *Energy Procedia* **2016**, *101*, 941–947. [[CrossRef](#)]
25. Akkurt, G.; Aste, N.; Borderon, J.; Buda, A.; Calzolari, M.; Chung, D.; Costanzo, V.; Del Pero, C.; Evola, G.; Cardenas, H.E.H.; et al. Dynamic thermal and hygrometric simulation of historical buildings: Critical factors and possible solutions. *Renew. Sustain. Energy Rev.* **2019**, *118*, 109509. [[CrossRef](#)]
26. Savoyat, J.; Johannes, K.; Virgone, J. Integration of thick wall in TRNSYS simulation. In Proceedings of the 30th ISES Biennial SWC 2011: ISES Solar World Congress, Kassel, Germany, 28 August–2 September 2011.
27. UNI EN ISO 7730; Determinazione degli Indici PMV e PPD e Specifica delle Condizioni di Benessere Termico. UNI (Ente Nazionale Italiano di Unificazione): Milan, Italy, 1997.
28. Cheung, T.; Schiavon, S.; Parkinson, T.; Li, P.; Brager, G. Analysis of the accuracy on PMV–PPD model using the ASHRAE Global Thermal Comfort Database II. *Build. Environ.* **2019**, *153*, 205–217. [[CrossRef](#)]
29. Buratti, C.; Ricciardi, P. Adaptive analysis of thermal comfort in university classrooms: Correlation between experimental data and mathematical models. *Build. Environ.* **2009**, *44*, 674–687. [[CrossRef](#)]
30. Buonomano, A.; Calise, F.; Ferruzzi, G.; Palombo, A. Dynamic energy performance analysis: Case study for energy efficiency retrofits of hospital buildings. *Energy* **2014**, *78*, 555–572. [[CrossRef](#)]
31. Ascione, F.; Bianco, N.; De Masi, R.F.; Vanoli, G.P. Rehabilitation of the building envelope of hospitals: Achievable energy savings and microclimatic control on varying the HVAC systems in Mediterranean climates. *Energy Build.* **2013**, *60*, 125–138. [[CrossRef](#)]
32. ISO 9869-1; Thermal Insulation—Building Elements—In situ Measurement of Thermal Resistance and Thermal Transmittance. ISO (International Organization for Standardization): Geneva, Switzerland, 2014.
33. UNI EN ISO 6946; Building Components and Building Elements—Thermal Resistance and Thermal Transmittance—Calculation methods. UNI (Ente Nazionale Italiano di Unificazione): Milan, Italy, 2017.
34. TRNSYS 17—A TRaNsient SYstem Simulation Program, User Manual; Version 17.02; Solar Energy Laboratory: University of Wisconsin: Madison, WI, USA, 2012.
35. TRNSYS3D, TRNSYS Includes TRNSYS3D—A plugin for SketchUp™; University of Wisconsin: Madison, WI, USA, 2012.
36. TRNSYS 17—A TRaNsient SYstem Simulation Program, User Manual; Version 17.02; Multizone Building Modeling with Type56 and TRNBuild, Solar Energy Laboratory; University of Wisconsin: Madison, WI, USA, 2012; Volume 5.
37. ISO 7730; Ergonomics of the Thermal Environment—Analytical Determination and Interpretation of Thermal Comfort using Calculation of the PMV and PPD Indices and Local Thermal Comfort Criteria. ISO International Organization for Standardization): Geneva, Switzerland, 2005.
38. ASHRAE Standard 62.1-2013; Ventilation for Acceptable Indoor Air Quality; ASHRAE (American Society of Heating, Refrigerating and Air-Conditioning Engineers): Atlanta, GA, USA, 2013.
39. UNI EN 12207; Windows and Doors—Air Permeability—Classification. UNI (Ente Nazionale Italiano di Unificazione): Milan, Italy, 2017.

40. EN 12464-1; Light and Lighting—Lighting of Work Places Part 1: Indoor Work Places. CEN (European Committee for Standardization): Brussels, Belgium, 2011.
41. Servizio Integrato Agrometeorologico della Regione Lazio (SIARL). Available online: <https://www.siarl-lazio.it/index.asp> (accessed on 13 August 2022).
42. Italian Republic. DPR 26/08/1993, n. 412 (G. U. n.96 del 14/10/1993), *Regolamento Recante Norme per la Progettazione, l'Installazione, l'Esercizio e la Manutenzione degli Impianti Termici degli Edifici ai Fini del Contenimento dei Consumi di Energia, in Attuazione dell'art.4, Comma 4, della Legge 9 Gennaio 1991, n. 10.*; Gazzetta Ufficiale: Rome, Italy, 1993.

Disclaimer/Publisher's Note: The statements, opinions and data contained in all publications are solely those of the individual author(s) and contributor(s) and not of MDPI and/or the editor(s). MDPI and/or the editor(s) disclaim responsibility for any injury to people or property resulting from any ideas, methods, instructions or products referred to in the content.